JACS
JOURNAL OF THE AMERICAN CHEMICAL SOCIETY
Article
Cite This: J. Am. Chem. Soc. 2018, 140, 11020−11028
pubs.acs.org/JACS

Self-Catalytic Reaction of SO_3 and NH_3 To Produce Sulfamic Acid and Its Implication to Atmospheric Particle Formation

Hao Li,[†,‡,#] Jie Zhong,[‡,#] Hanna Vehkamäki,[○] Theo Kurtén,[§] Weigang Wang,[∥] Maofa Ge,[∥] Shaowen Zhang,[†] Zesheng Li,[†] Xiuhui Zhang,*[,†] Joseph S. Francisco,*[,‡] and Xiao Cheng Zeng*[,◆,‡,⊥]

[†]Key Laboratory of Cluster Science, Ministry of Education of China, School of Chemistry and Chemical Engineering, Beijing Institute of Technology, Beijing 100081, P. R. China

[‡]Department of Chemistry, University of Nebraska-Lincoln, Lincoln, Nebraska 68588, United States

[§]Institute for Atmospheric and Earth System Research/Chemistry and [○]Institute for Atmospheric and Earth System Research/Physics, University of Helsinki, PO Box 64 (Gustaf Hällströmin katu 2a), FI-00014 Helsinki, Finland

[∥]Beijing National Laboratory for Molecular Sciences (BNLMS), State Key Laboratory for Structural Chemistry of Unstable and Stable Species, Institute of Chemistry, Chinese Academy of Sciences, 100190 Beijing, China

[⊥]Beijing Advanced Innovation Center for Soft Matter Science and Engineering, Beijing University of Chemical Technology, Beijing 100029, China

Supporting Information

ABSTRACT: Sulfur trioxide (SO_3) is one of the most active chemical species in the atmosphere, and its atmospheric fate has profound implications to air quality and human health. The dominant gas-phase loss pathway for SO_3 is generally believed to be the reaction with water molecules, resulting in sulfuric acid. The latter is viewed as a critical component in the new particle formation (NPF). Herein, a new and competitive loss pathway for SO_3 in the presence of abundant gas-phase ammonia (NH_3) species is identified. Specifically, the reaction between SO_3 and NH_3, which produces sulfamic acid, can be self-catalyzed by the reactant (NH_3). In dry and heavily polluted areas with relatively high concentrations of NH_3, the effective rate constant for the bimolecular SO_3−NH_3 reaction can be sufficiently fast through this new loss pathway for SO_3 to become competitive with the conventional loss pathway for SO_3 with water. Furthermore, this study shows that the final product of the reaction, namely, sulfamic acid, can enhance the fastest possible rate of NPF from sulfuric acid and dimethylamine (DMA) by about a factor of 2. An alternative source of stabilizer for acid−base clustering in the atmosphere is suggested, and this new mechanism for NPF has potential to improve atmospheric modeling in highly polluted regions.

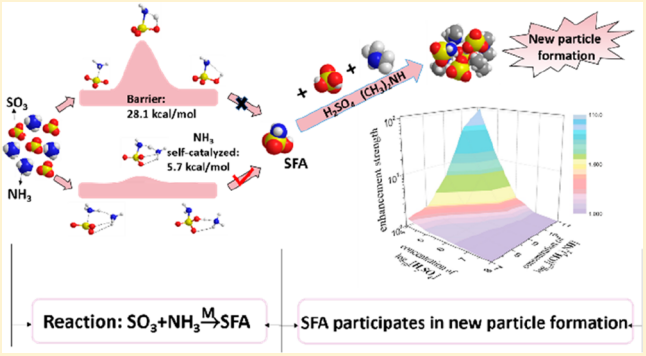

INTRODUCTION

Sulfur trioxide (SO_3) is a major air pollutant[1−5] and is mainly produced by the gas-phase oxidation of SO_2.[6,7] As a highly reactive gas[8] and one of the most common acid oxides, SO_3 can lead to both acid rain and atmospheric aerosol[9−13] and thus has important implications for regional climate and human health.[14−19] The reaction between SO_3 and water (H_2O) has been generally considered as the dominant pathway for the loss of SO_3 because the H_2O concentration is $\sim 10^{17}$ molecules cm^{-3} in the boundary layer, which is several orders of magnitude greater than that of other condensable gases.[20] The relevant reaction equation can be described by reaction 1:

$$SO_3 + H_2O \xrightarrow{M} H_2SO_4 \quad (1)$$

Both experimental and theoretical studies[21−26] indicate that a facilitator molecule M, acting as a catalyst, is required. For example, previous experiment study by Jayne et al.[23] showed that reaction 1 exhibits second-order dependence on water vapor concentration, and other previous theoretical studies[22] indicated the addition of a second water molecule could substantially lower the activation barrier. More recently, sulfuric acid (SA)[24] or other atmospheric molecules (such as formic acid[25] or ammonia[26]) make the reactions barrierless and thus significantly fast. However, in highly polluted regions, the concentration of NH_3 can reach 105.0 $\mu g\ m^{-3}$ (or $\sim 3.7 \times 10^{12}$ molecules cm^{-3}).[27] Furthermore, in relatively dry conditions or at lower temperatures, e.g., in the winter, the

Received: May 11, 2018
Published: August 8, 2018

DOI: 10.1021/jacs.8b04928
J. Am. Chem. Soc. 2018, 140, 11020−11028

concentration of gas-phase water molecules is drastically reduced.[13] Hence, SO_3 may react with NH_3 before reacting with H_2O.

The possibility of an SO_3−NH_3 reaction was previously studied in the laboratory, and its effective rate coefficient was detected to be 10^{-12}−10^{-10} cm^3 $molecule^{-1}$ s^{-1} at NH_3 concentration of 10^{11}−10^{13} molecules cm^{-3}.[28−32] Such unexpectedly high values of the rate coefficient are similar to those of SO_3 and water dimer reaction (10^{-11}−10^{-10} cm^3 $molecule^{-1}$ s^{-1}),[21−23,33] implying that the reaction with NH_3 might be an important sink of SO_3. A Fourier-transform infrared spectroscopy (FTIR) study by Hirota et al.[30] showed that with NH_3 the product from the reaction of SO_3 was sulfamic acid (H_2NSO_3H, SFA). Previous theoretical studies[34,35] predicted that a direct SO_3−NH_3 reaction was kinetically unfavorable because of the high reaction barrier (28.6 kcal/mol). The discrepancy between theoretical and experimental results suggests that this reaction might require a facilitator molecule M, as in reaction 2:

$$SO_3 + NH_3 \xrightarrow{M} H_2NSO_3H \tag{2}$$

Thus, it is important to determine whether reaction 2 entails a much lower reaction barrier with either another NH_3 molecule or the SFA molecule as a catalyst, and also important to elucidate the underlying reaction mechanism.

From the perspective of its structure, SFA possesses two functional groups: a sulfonic acid and an amino group. Both groups can act as hydrogen donors and acceptors to interact with atmospheric particle precursors as proven by previous works.[36−39] Furthermore, in the experiment performed by Lovejoy et al.,[29] SFA was observed to cluster efficiently with itself and SA, indicating its potential for aerosol new particle formation (NPF). Although several compounds have been identified in promoting NPF process, they are mostly correlated with special environment, for example, highly oxidized multifunctional organic molecules (HOMs) mostly in forest, rural, and urban areas,[40−43] iodic acid (HIO_3) in coastal area and open ocean region,[44] and methanesulfonic acid (MSA) mostly in marine region.[45] A main question that we intend to address here is whether SFA produced by the reaction between SO_3 and NH_3 is capable of enhancing the nucleation of SA and base (i.e., ammonia or amine) molecular clusters, in view of that the latter species have been recognized as dominant precursors in highly polluted areas, especially in some megacities in Asia.[46−53]

In this work, using high-level theoretical methods, we first studied the reaction between SO_3 and NH_3 to form SFA with the reactant (NH_3) or product (SFA) being considered as a self- or autocatalyst. Next, we used the Atmospheric Clusters Dynamic Code (ACDC)[54] to investigate how the product (SFA) is involved in SA-dimethylamine (SA-DMA)-based cluster formation. Particular attention of this work is placed on the study of (1) the possibility of the SO_3 and NH_3 reaction functioning as an important loss pathway in highly polluted areas with high NH_3 concentrations and (2) the fate of the product in atmospheric NPF and the influence of various environmental conditions.

METHODS

Quantum Chemical Calculation. All density functional theory (DFT) calculations were performed with using Gaussian 09[55] software packages. For all reactions involving SO_3 and NH_3, structure optimization and subsequent frequency analysis of the stationary points were carried out at the M06-2X/6-311++G(3df,3pd) level of theory. Several previous studies[36−39,56] have shown that the M06-2X functional is an accurate DFT method for computing thermochemistry, kinetics, and noncovalent interactions involving the main-group elements. Intrinsic reaction coordinate (IRC) was also calculated to ensure the correct transition states for the products and reactants. Single-point energies for the stationary points were computed using the ORCA 3.03 Package[57] to obtain more reliable energies. To this end, the explicitly correlated coupled cluster (CCSD(T)-F12)[58] method with the cc-pVDZ-F12 basis set[59] and appropriate auxiliary basis sets were used.

For the chemical processes involving interactions between SFA and other precursors resulting in particle formation, a systematic sampling technique was used to search for the global minima of the molecular clusters. In the first step, a thousand structures are autogenerated using the ABCluster[60] software with the TIP4P[61,62] model for water molecules and the CHARMM[63] force field for others; these structures were then preoptimized based on the semiempirical method (PM7) with Mopac2016.[64,65] Next, up to 100 low-energy conformations were reoptimized using the M06-2X/6-31+G* level of theory to determine the ten lowest-lying structures, followed by another optimization with using the larger 6-311++G(3df,3pd) basis set to determine the global minimum. The Cartesian coordinates and the corresponding formation Gibbs free energy of the stable clusters are summarized in the Supporting Information.

Atmospheric Clusters Dynamic Code (ACDC) Model. The ACDC[54] kinetic model with the MATLAB-R2013a[66] program is used to compute the time evolution of formation rates and growth paths of the clusters. For a given set of atmospheric clusters, the code can be used to solve the birth−death equations (see eq 3 below) with calculated formation free energies (based on other theoretical method) as the inputs. The overall process accounts for all possible collision and evaporation of the relevant clusters. Specifically, the birth−death equation is written as

$$J = \frac{dc_i}{dt} = \frac{1}{2}\sum_{j<i}\beta_{j,(i-j)}c_j c_{(i-j)} + \sum_j \gamma_{(i+j)\to i}c_{i+j} - \sum_j \beta_{i,j}c_i c_j - \frac{1}{2}\sum_{j<i}\gamma_{i\to j}c_i + Q_i - S_i \tag{3}$$

where J refers to the cluster formation rate, i (or j) is a molecule or a cluster, c_i stands for the concentration of i, $\beta_{i,j}$ and $\gamma_{i+j\to i}$ are the collision coefficient of i with j or the evaporation coefficient of $i + j$ cluster evaporating into i and j, respectively. Q_i, set to be zero in the present study, is the possible other source of i. S_i represents the sink term of i.

The collision coefficient $\beta_{i,j}$ is based on the kinetic gas theory[67,68] and eq 4:

$$\beta_{i,j} = \left(\frac{3}{4\pi}\right)^{1/6}\left(\frac{6k_bT}{m_i} + \frac{6k_bT}{m_j}\right)^{1/2}(V_i^{1/3} + V_j^{1/3})^2 \tag{4}$$

where m_i and V_i are the mass and volume of i, and similarly, m_j and V_j are the mass and volume of j, respectively, which are calculated via eq 5

$$V = \left(\frac{4}{3}\right)\pi(r)^3 \tag{5}$$

where r is the molecular radius derived by using Multiwfn software.[69] More details can be found from our previous paper.[70]

The evaporation coefficient $\gamma_{(i+j)\to i}$ was calculated using the formation Gibbs free energies of the given clusters and eq 6

$$r_{(i+j)\to i} = \beta_{i,j}\frac{c_i^e c_j^e}{c_{i+j}^e} = \beta_{i,j}c_{ref}\exp\left\{\frac{\Delta G_{i+j} - \Delta G_i - \Delta G_j}{k_bT}\right\} \tag{6}$$

where c_i^e refers to the equilibrium concentration of i, ΔG_i is the formation free energy of i, and c_{ref} represents the monomer

DOI: 10.1021/jacs.8b04928
J. Am. Chem. Soc. 2018, 140, 11020−11028

concentration of the reference vapor at a pressure of 1 atm, which is the pressure at which the Gibbs free energies are determined.

Generally, the simulation system is regarded as an "$a \times b$" box, where a or b is the maximum number of acid or base molecules of the clusters, respectively. Here, the cluster size of the simulated systems was set to be 3 × 2, containing $(SFA)_x(SA)_y(DMA)_z$ (where the sum of x and y from 0 to 3, z from 0 to 2) clusters. The mobility diameter of the largest cluster is 1.7 nm, which is chosen because the NPF rates typically use this standard during experimental measurement.[71] Among these clusters, only the clusters including an equal numbers of base and acid molecules or the clusters with smaller numbers of base than acid molecules were considered, as only these clusters have the potential to further grow into larger sizes.[72] In addition, considering the formation Gibbs free energy (Table S1) and evaporation rates (Table S2), the clusters containing SA and DMA molecules and an SFA molecule are the most stable and are therefore allowed to grow to larger clusters, thereby contributing to the rate of NPF. Given the above considerations, clusters $(SA)_3 \cdot (DMA)_3$ and $SFA \cdot (SA)_2 \cdot (DMA)_3$ are set as the boundary clusters. Moreover, the coagulation sink coefficient is set to be 5×10^{-2} s^{-1} in the case of polluted areas.[73−75]

RESULTS AND DISCUSSION

Reactant as Self-Catalyst and Product as Autocatalyst. A previous theoretical study[34] showed that the direct reaction between SO_3 and NH_3 without a catalyst is not a plausible path for SFA formation due to a high reaction barrier (Figure 1a). The high barrier is a consequence of large ring tension of the rather closed four-membered ring transition-state geometry, making SFA formation kinetically unfavorable. However, previous experimental studies[28,29] indicated that the bimolecular rate coefficient for the SO_3−NH_3 reaction can reach ∼10^{-10} cm^3 $molecule^{-1}$ s^{-1}. Such a high reaction rate coefficient reflects a fast and easy reaction. The apparent inconsistency between experimental measurement and theoretical prediction suggests that the reaction between SO_3 and NH_3 may involve a catalyst. Thus, we first examine the SFA formation from the SO_3 and NH_3 reaction with either the NH_3 reactant or the SFA product as a catalyst. As shown in Figure 1b, with the reactant (NH_3) acting as a catalyst, the reaction barrier is substantially lower than that of the direct reaction (Figure 1a). Reactions starting with the formation of different dimers among two of three molecules (SO_3, NH_3, and NH_3 molecules) were examined, and the $SO_3 \cdot NH_3$ heterodimer was expected to be the best candidate due to its most negative Gibbs free energy of formation (-10.0 kcal mol^{-1}) among the possible dimers. Next, the reaction continues to yield a prereactive complex C2 with a formation free energy of −12.4 kcal mol^{-1}, followed by the formation of a hydrogen-bonded complex P2 via TS2 transition state, with a free energy barrier of 5.7 kcal mol^{-1}. The NH_3 molecule in TS2 acts as a double donor and a single acceptor of hydrogen to form a steric network with an $SO_3 \cdot NH_3$ heterodimer through van der Waals interactions. As a result, the ring strain of the transition state is reduced with increasing ring size from a four-membered ring structure to a cage-like hydrogen-bonding network; the associated energy barrier is significantly lower than that without the self-catalyst. Hence, the reactant self-catalysis mechanism for the SO_3−NH_3 reaction is predicted.

In addition to the reactant (NH_3) self-catalysis mechanism, the SFA autocatalysis mechanism (Figure 1c) can also facilitate the formation of SFA with high efficiency. The reaction barrier involved is 9.0 kcal mol^{-1}, which is also much lower than that without the autocatalyst (Figure 1a). This autocatalysis reaction can, in principle, begin with three primary paths

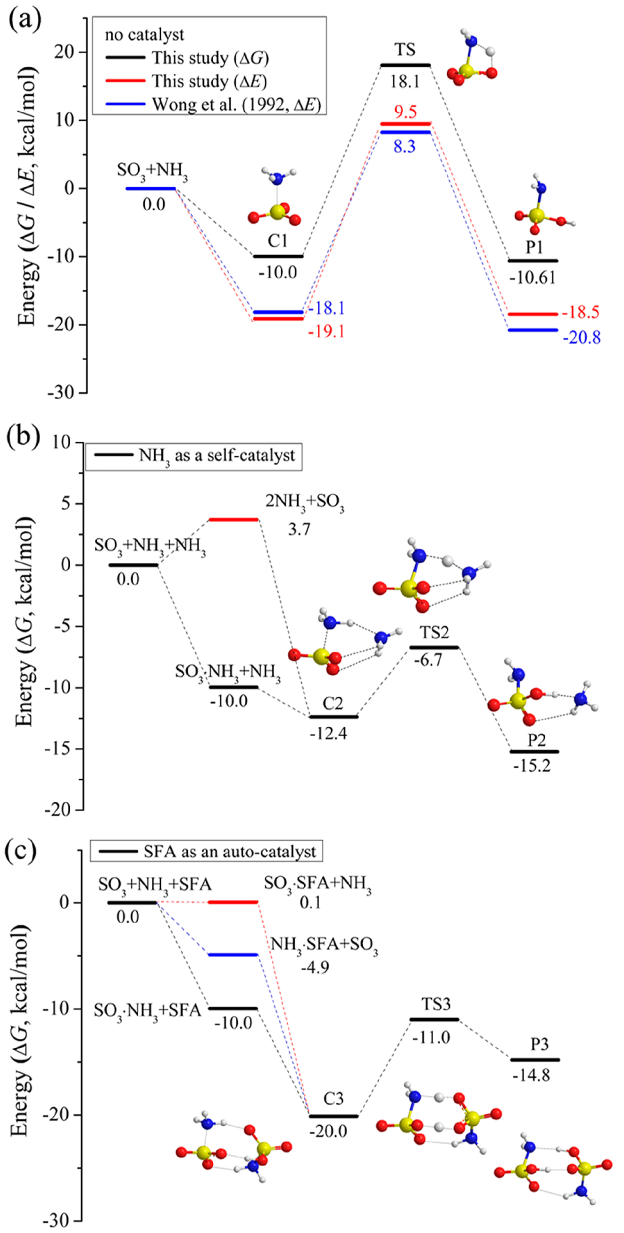

Figure 1. Potential energy surfaces for the reaction of SO_3 and NH_3 with (a) no catalyst; (b) NH_3 as a self-catalyst; and (c) SFA as an autocatalyst. Hydrogen, oxygen, sulfur, and nitrogen atoms are represented by gray, red, yellow, and blue spheres, respectively. C, TS, and P refer to prereaction complex, transition state, and product, respectively.

involving the bimolecular collision between an NH_3 molecule and an SO_3 molecule, a collision between an SO_3 molecule and an SFA molecule, or a collision between an SFA molecule and an NH_3 molecule. However, Figure 1c shows that the first path is most likely due to the greater stability of $SO_3 \cdot NH_3$ heterodimer among the three possible first formed dimers. Thus, the reaction starting with the formation of an $SO_3 \cdot NH_3$ heterodimer, followed by the formation of a prereactive complex C3, with a formation free energy of −20.0 kcal mol^{-1} (much lower than the value for C2 (−12.4 kcal mol^{-1})) indicates greater binding ability of the $SO_3 \cdot NH_3$ heterodimer with product SFA than with reactant NH_3. Finally, the complex C3 proceeds via transition state TS3 to form a hydrogen-bonding complex P3. In the mechanism above, the product

DOI: 10.1021/jacs.8b04928
J. Am. Chem. Soc. 2018, 140, 11020−11028

Table 1. Calculated Forward/Reverse Rate Coefficients (k_7/k_{-7} and k_8/k_{-8}), the Unimolecular Rate Constant (k_9), the Concentration of Catalyst ([M]), and the Reaction Rate Constant (k) for the Reaction of SO_3 + NH_3 without a Catalyst, with Reactant NH_3 as a Self-catalyst, and the Product SFA as an Autocatalyst

	without catalyst	NH_3 self-catalysis	SFA autocatalysis (under laboratory conditions)	SFA autocatalysis (under atmospheric conditions)
k_7 (cm^3 $molecule^{-1}$ s^{-1})	4.35×10^{-10}	4.35×10^{-10}	4.35×10^{-10}	4.35×10^{-10}
k_{-7} (s^{-1})	5.32×10^{2}	5.32×10^{2}	5.32×10^{2}	5.32×10^{2}
k_8 (cm^3 $molecule^{-1}$ s^{-1})		4.96×10^{-10}	3.96×10^{-10}	3.96×10^{-10}
k_{-8} (s^{-1})		1.99×10^{8}	4.12×10^{2}	4.12×10^{2}
k_9 (s^{-1})	1.64×10^{-8}	4.46×10^{8}	1.53×10^{6}	1.53×10^{6}
[M] (molecules cm^{-3})		10^{9}–10^{13}	10^{11}–10^{15}	10^{4}–10^{8}
k (cm^3 $molecule^{-1}$ s^{-1})	1.33×10^{-20}	2.78×10^{-13} to 2.72×10^{-10}	3.01×10^{-11} to 4.34×10^{-10}	3.23×10^{-18} to 4.34×10^{-14}
effective rate constant[28,29]	10^{-12}–10^{-10} (cm^3 $molecule^{-1}$ s^{-1}) (laboratory conditions)			

SFA molecule, as an autocatalyst, mediates the formation of the N–S covalent bond by transfer of a proton from NH_3 to an oxygen atom of SO_3. These computations indicate that either the reactant or product can function as a catalyst to make the reaction between SO_3 with NH_3 much more energetically accessible, as observed in previous experiments.

Reaction Rate of the SO_3–NH_3 Reaction. Given the self-catalysis ability of reactant NH_3 and the autocatalysis ability of product SFA, it is important to examine the reaction rate of the SO_3 and NH_3 reaction and compare this rate with that of the SO_3 and H_2O reaction to determine if the reaction with NH_3 is an important loss pathway for SO_3. Kinetic calculations are carried out based on conventional transition-state theory (TST)[24,25,76−78] to evaluate the effects of NH_3 and SFA on the rate constants for the reaction between SO_3 and NH_3. Besides, the TST with Wigner tunneling correction is also considered (see Table S3), and the results indicate that the tunneling effect has little impact on the reaction rate constant. As previously described, the self- or autocatalyzed reaction mainly proceeds via the following reaction sequence:

$$SO_3 + NH_3 \rightarrow SO_3{-}NH_3 \quad (7)$$

$$SO_3{-}NH_3 + M \rightarrow SO_3{-}NH_3{-}M \quad (8)$$

$$SO_3{-}NH_3{-}M \rightarrow SFA{-}M \quad (9)$$

$$SFA{-}M \rightarrow SFA + M \quad (10)$$

where M represents the catalyst (reactant NH_3 or product SFA). The energy profiles for reaction steps 7–10 shown in Figure 1b,c indicate that reaction 9 is the rate-determining step. Applying the steady-state approximation to the prereactive complex and assuming that the complex is in equilibrium with the reactant, we derive the following equation:

$$r = \frac{\mathrm{d}[SFA]}{\mathrm{d}t} = \frac{k_7}{(k_{-7} + k_8[M])} \times \frac{k_8}{(k_{-8} + k_9)} \times k_{10}[SO_3][NH_3][M] \quad (11)$$

where k_7/k_{-7} and k_8/k_{-8} denote the ratio of the forward/reverse rate coefficients for reactions 7 and 8, respectively, and k_9 is the unimolecular rate constant for reaction 9. Thus, the rate constant k for reaction 2 can be expressed as

$$k = \frac{r}{[SO_3][NH_3]} = \frac{k_7}{(k_{-7} + k_8[M])} \times \frac{k_8}{(k_{-8} + k_9)} \times k_{10}[M] \quad (12)$$

where k can be viewed as a measure of the relative efficiency of different catalysts because their concentrations are also included in eq 12.

For SFA, wide concentration ranges from 10^{11} to 10^{15} molecules cm^{-3} and from 10^{4} to 10^{8} molecules cm^{-3} are examined, respectively, reflecting an SO_3 concentration of 10^{9}–10^{13} molecules cm^{-3} examined in the laboratory, and a concentration of 10^{0}–10^{5} molecules cm^{-3} observed in the atmosphere (see Tables S4 and S5). The computed rate constants for both conditions are presented in Table 1. Without considering the catalyst, the rate constant k is ~10^{-20} cm^3 $molecule^{-1}$ s^{-1}, which is too small for the reaction to occur. Under typical laboratory conditions, the reaction rate constant k for the SO_3 and NH_3 reaction catalyzed by either reactant NH_3 or product SFA increases significantly, and the rate constant can be as high as 10^{-10} cm^3 $molecule^{-1}$ s^{-1}, consistent with the experimentally measured value.[28,29] Both reactant self-catalysis and product autocatalysis mechanisms can explain the observed spectral signals of SFA formed from SO_3 (in the presence of SO_2 and O_2) and NH_3 in the laboratory.[30] However, considering that the product SFA concentration is significantly lower than that observed in the experiment (10^{4} to 10^{8} molecules cm^{-3} in Table S5), the high reaction rate constant (10^{-10} cm^3 $molecule^{-1}$ s^{-1}) would be difficult to attain through SFA autocatalysis alone. Thus, we expect that the reaction through NH_3 self-catalysis is the major sink of SO_3 in areas with abundant NH_3 in the atmosphere.

The competition between the two reactions, one between SO_3 and NH_3 and the other between SO_3 and H_2O, also warrants investigation given that the latter reaction is generally considered as the dominant loss process of SO_3. The rate constant of the SO_3 and $(H_2O)_2$ reaction is 10^{-11}–10^{-10} cm^3 $molecule^{-1}$ s^{-1} for H_2O-involved self-catalysis reaction.[26] Under normal atmospheric conditions, the concentration of $(H_2O)_2$ (~10^{14} molecules cm^{-3})[79,80] is much higher than that of NH_3; hence, the reaction with H_2O will be the dominant sink pathway for SO_3. However, in highly polluted areas with relatively dry conditions, the concentration of NH_3 can be comparable with that of $(H_2O)_2$; thus, the reaction between SO_3 and NH_3 can potentially compete with the reaction between SO_3 and H_2O (ratios of the rates of the two reactions are given in Tables S6–S9). Note also that Bandyopadhyay et

DOI: 10.1021/jacs.8b04928
J. Am. Chem. Soc. 2018, 140, 11020–11028

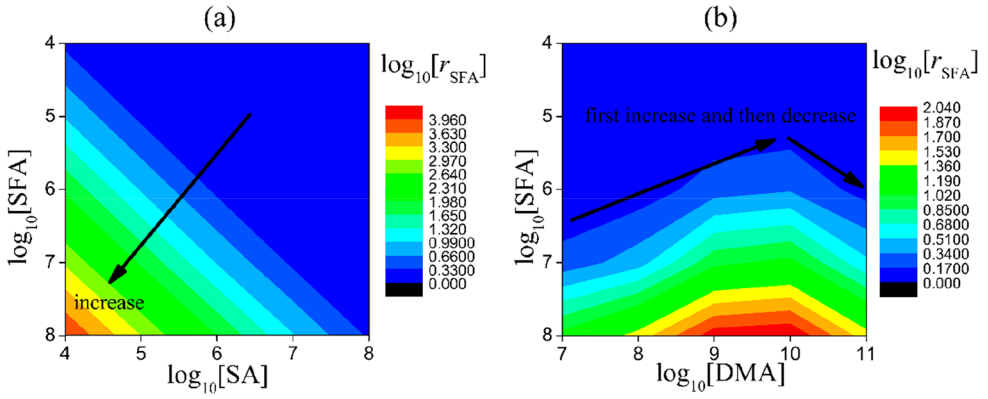

Figure 2. (a) Cluster formation rates ratio (r_{SFA}) versus the logarithm of [SA] and [SFA] at [DMA] = 10^9 molecules cm^{-3} and (b) the logarithm of [DMA] and [SFA] (T = 278 K and $10^4 \leq$ [SFA] $\leq 10^8$ molecules cm^{-3}). The color bars are values for $\log_{10}[r_{SFA}]$.

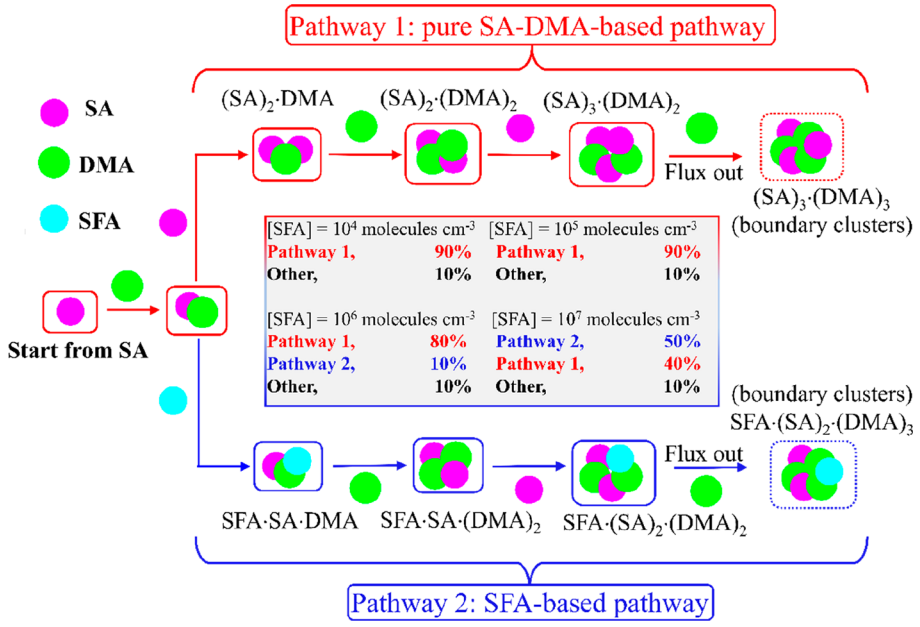

Figure 3. Main pathways and the corresponding mechanism of cluster growth within the cluster size range considered, at T = 278 K, [SA] = 10^6 molecules cm^{-3}, [DMA] = 10^9 molecules cm^{-3}, and $10^4 \leq$ [SFA] $\leq 10^8$ molecules cm^{-3}. The blue and red fluxes represent the growth pathways of SFA-contained clusters and pure SA-DMA-based clusters, respectively.

al.[26] suggested that the SO_3 + H_2O reaction could also be effectively catalyzed by NH_3 molecule, with a high reaction rate constant (~10^{-4} cm^3 molecule^{-1} s^{-1}) for SO_3 and $H_2O{\cdot}NH_3$ reaction. Given that the $H_2O{\cdot}NH_3$ concentration is several orders of magnitude lower than that of $(H_2O)_2$ or NH_3, the reaction of SO_3 and NH_3 could also be competitive with that of SO_3 and $H_2O{\cdot}NH_3$ (ratios of the rates of the two reactions are given in Tables S10–S12).

Atmospheric Implication: Enhancement Effect of SFA on NPF. Knowing that the formation of SFA becomes an important and competitive loss pathway for SO_3 in the atmosphere with a high concentration of NH_3, we performed ACDC simulations to achieve a deeper understanding of the influence of SFA on SA-DMA-based molecular clustering, a known source for NPF.[48] The ratio (r_{SFA}) of formation rates with SFA to the rate without SFA is given by eq 13 for temperature T = 298, 278, and 258 K, corresponding to the temperature conditions in the boundary layer and in the lower troposphere:[81]

$$r_{SFA} = \frac{J([SFA] = x, [SA] = y, [DMA] = z)}{J([SA] = y, [DMA] = z)} \quad (13)$$

where [SFA], [SA], and [DMA] stand for SFA, SA, and DMA concentrations, respectively. [SFA] was varied from 10^4 to 10^8 molecules cm^{-3} (Table S5); the 10^4–10^8 molecules cm^{-3} of [SA] and 10^7–10^{11} molecules cm^{-3} of [DMA] are chosen since these values are the typical observed values in the atmosphere.[82−84] The enhancement factor (r_{SFA}) at three different temperatures (Tables S14–S16, Figures S1–S2; Figure 2) is always equal to or larger than 1.0, reflecting the enhancement ability of SFA on the SA-DMA-based system. At 278 K, for example, the dependence of the enhancement factor r_{SFA} on [SFA], [SA], and [DMA] is shown in Figure 2. The r_{SFA} increases with increasing [SFA] and reaches as high as 10^5 at [SFA] = 10^8 molecules cm^{-3} (Figure 2a,b) with low [SA] of 10^4 molecules cm^{-3}. Generally, high absolute cluster formation rates relevant to observed atmospheric NPF[46,50,84,85] are associated with fairly low values of r_{SFA} (Tables S14–S16). However, the enhancement effect of SFA may still be

DOI: 10.1021/jacs.8b04928
J. Am. Chem. Soc. 2018, 140, 11020−11028

Scheme 1. Suggested Scheme of the Important Loss Pathway for SO_3 in Highly Polluted Atmosphere with a High NH_3 Concentration

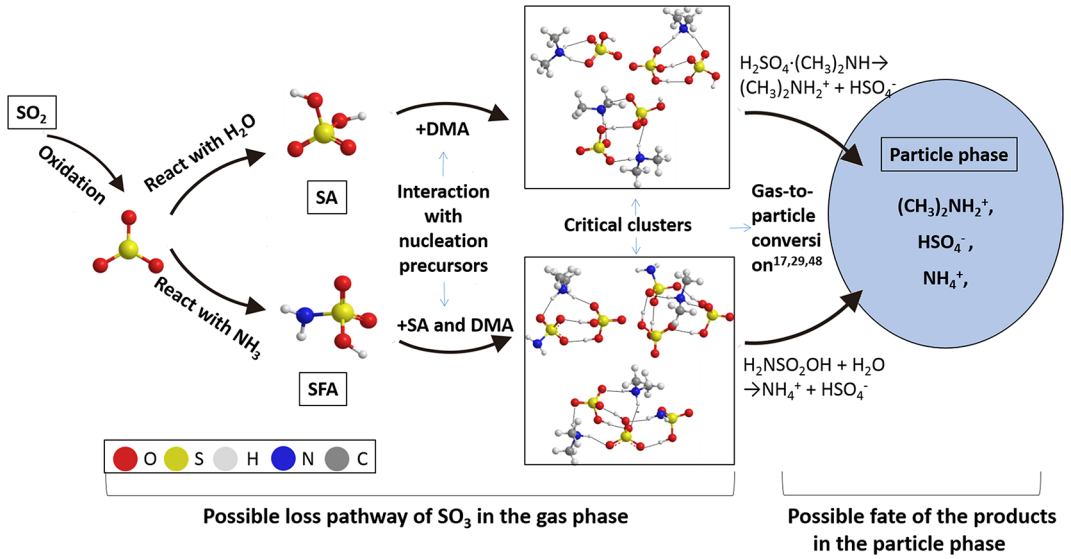

significant in many atmospherically relevant conditions; for example at [SA] = 10^6 and [DMA] = 10^{10} molecules cm^{-3}, an SFA concentration of 10^6 leads to an enhancement factor of 2 at T = 298 K and an overall formation rate of J = 115 cm^{-3} s^{-1}.

Moreover, r_{SFA} decreases as [SA] increases, as shown in Figure 2a, likely due to the stronger binding between SA and DMA than between SFA and DMA (or between SFA and SA). At a constant concentration of SFA and DMA, increasing SA leads to increased SA-DMA clustering at the expense of SFA-containing clusters, and also to decreased r_{SFA}, even as the overall particle formation rate increases. The influence of [DMA] on the ratio r_{SFA} shows a different trend compared with that of [SA] (Figure 2b), where r_{SFA} increases first as [DMA] changes from 10^7 to 10^{10} molecules cm^{-3}. This might be due to the increased hydrogen bonding interaction between acidic molecule SFA and the added base molecule DMA. As such, with the increase of [DMA] to 10^9 molecules cm^{-3}, saturation of hydrogen bonding interaction is reached for SFA, thus resulting in the maximum enhancement strength, whereas with further increase of [DMA], r_{SFA} decreases as [DMA] changes from 10^{10} to 10^{11} molecules cm^{-3}. This is because the hydrogen bonds between SFA and SA could be disrupted by the added DMA molecules, leading to the decreased interaction between SFA with other molecules, thereby decreasing the r_{SFA}. This phenomenon could be a common feature for the system involving acidic compounds, such as HMSA and glycolic acid.[37,86] Furthermore, the variation of enhancement factor with the increase of [DMA] in the presence of NH_3 is further examined (Figure S3). The results show that the enhancement factor of SFA first increases and then decreases with increasing [DMA], while the relatively high [NH_3] of 10^{10} to 10^{11} molecules cm^{-3} has only a minor effect.

To further identify the mechanism by which SFA offers its enhancement effect, the main pathways of cluster growth were traced using ACDC. The principal growth paths of SFA-SA-DMA-based clusters at different [SFA] with median [SA] of 10^6 molecules cm^{-3} and [DMA] of 10^9 molecules cm^{-3} at 278 K are shown in Figure 3. At [SFA] = 10^4 and 10^5 molecules cm^{-3}, SFA molecules do not substantially contribute to the cluster growth, and the pathway just shows the growth of pure SA-DMA-based clusters. These results are consistent with those in Figure 2a, where SFA also shows little effect on cluster formation rate. When [SFA] is increased to 10^6 molecules cm^{-3}, SFA appears to be responsible for an alternative pathway (marked by blue lines in Figure 3). In this pathway, the initially generated SFA-containing cluster is SFA·SA·DMA, formed by collision of SFA with a pre-existing SA·DMA cluster. Thereafter, the SFA·SA·DMA cluster grows via a base-stabilization mechanism, and each addition of an acid molecule is stabilized by one additional DMA molecule, following the sequence of acid−base pairs: SFA·SA·DMA → SFA·SA·$(DMA)_2$ → SFA·$(SA)_2$·$(DMA)_2$ → flux out. In this case, the contribution of SFA is only 10%, while with the further increase of [SFA], its role becomes even more important. As shown in Figure 3, SFA plays a dominant role, and its contribution is substantially increased from 10% at [SFA] = 10^6 molecules cm^{-3} to 50% at [SFA] = 10^7 molecules cm^{-3}.

SFA molecule shows an ability to directly participate in the cluster formation, suggesting that SFA can be a "participator" in facilitating NPF. Contrary to other common acid species as reported in our recent works,[70,87,88] such organic acids, e.g., lactic acid and glyoxylic acid, and inorganic acids, e.g., nitric acid, can only be indirectly involved in the growth pathway, acting as a "transporter" (which initially participates and eventually evaporates). Note that, like SFA, another two species with sulfonic group, namely, methanesulfonic acid (MSA)[36] and hydroxymethanesulfonic acid (HMSA),[37] are also identified to directly participate in the cluster formation. However, depending on the formation source of these species, the MSA tends to promote NPF mainly on marine areas. Although HMSA is likely to participate in the process of NPF,[37] the formation source of HMSA in the gas phase is still an open question, and its atmospheric concentration still needs to be explored to confirm its roles in NPF. Overall, among the three species containing sulfonic groups, the SFA represents the most compiling species toward NFP in highly polluted areas with high NH_3 concentration.

The environmental fate of SFA is likely to hydrolyze to ammonium sulfate in the aqueous phase, as previously

DOI: 10.1021/jacs.8b04928
J. Am. Chem. Soc. 2018, 140, 11020−11028

reported.[10,30,31] Thus, the formation of SFA-containing molecular clusters, followed by reaction with water and hydrolysis to form ammonium sulfate, may constitute an alternate pathway to sulfate production in the particle phase (see Scheme 1). All the suggested mechanisms may also be extended to the other loss paths of SO_3 with other common bases, such as amines, which are also likely to contribute to the atmospheric sink of SO_3, especially in areas with high concentrations of the base gases. Hence, scenarios involving SFA and its analogues should be assessed on their role in atmospheric particle formation.

CONCLUSION

We have investigated the reaction of NH_3 with SO_3 to form SFA and the subsequent effect of SFA on NPF in highly polluted regions with high concentration of NH_3. The important chemistry found in this study is that, with self-catalysis by the reactant NH_3, the activation barrier for the SO_3−NH_3 reaction can be drastically lowered. Hence, at high NH_3 concentration, the effective reaction rate coefficient can reach $\sim 10^{-10}$ cm^3 molecule^{-1} s^{-1}, indicating that the reaction is sufficiently fast to be competitive with the conventional SO_3−H_2O reaction (effective rate constant of 10^{-11}−10^{-10} cm^3 molecule^{-1} s^{-1}). This newly identified self-catalyzed reaction provides a previously unreported loss pathway of SO_3 at relatively low H_2O concentration and high NH_3 concentration. Our study shows that the product of the self-catalyzed reaction, SFA, can directly participate in the SA-DMA-based cluster formation, thereby substantially enhancing the cluster formation rate. This new stabilization mechanism in acid−base clustering has important implication to the aerosol NPF in highly polluted regions with high concentrations of base species.

ASSOCIATED CONTENT

Supporting Information

The Supporting Information is available free of charge on the ACS Publications website at DOI: 10.1021/jacs.8b04928.

Formation Gibbs free energies and the sum of evaporation rates of the clusters; imaginary frequencies of the transition states and the Wigner tunneling correction factor of the reactions; possible concentration of SFA in the experiment and in the real atmosphere; ratio of reaction rate for SO_3 + NH_3 reaction and SO_3 + H_2O reaction under different [NH_3] and [H_2O]; formation Gibbs free energies and a sum of evaporation rates of the clusters containing SFA, SA DMA, and NH_3; enhancement strength of SFA; ratio of cluster formation rates as a function of the logarithm of [SA] and [DMA]; optimized geometries of key species involved in particle formation in gas-phase; ratio of cluster formation rates versus the logarithm of [DMA] (PDF)

AUTHOR INFORMATION

Corresponding Authors

*E-mail: zhangxiuhui@bit.edu.cn.
*E-mail: jfrancisco3@unl.edu.
*E-mail: xzeng1@unl.edu.

ORCID

Theo Kurtén: 0000-0002-6416-4931
Maofa Ge: 0000-0002-1771-9359
Zesheng Li: 0000-0002-6993-8414
Xiuhui Zhang: 0000-0001-9570-7882
Joseph S. Francisco: 0000-0002-5461-1486
Xiao Cheng Zeng: 0000-0003-4672-8585

Present Address

◆(J.S.F.): Department of Earth and Environmental Science and Department of Chemistry University of Pennsylvania, Philadelphia, PA 19104.

Author Contributions

#Authors contributed equally.

Notes

The authors declare no competing financial interest.

ACKNOWLEDGMENTS

We thank the Chinese National Natural Science Foundation (91544227, 21373025) and "the Fundamental Research Funds for the Central Universities". We also gratefully thank the useful help of Jonas Elm (Aarhus University). H.L. thanks CSC (China Scholarship Council). T.K. thanks the Academy of Finland for funding. H.V. thanks the European Research Council (Grant 692891-DAMOCLES) and the University of Helsinki, Faculty of Science ATMATH project for funding. We also acknowledge computation support of UNL Holland Computing Center.

REFERENCES

(1) Zhuang, Y.; Pavlish, J. H. *Environ. Sci. Technol.* **2012**, *46*, 4657.
(2) Chen, L.; Bhattacharya, S. *Environ. Sci. Technol.* **2013**, *47*, 1729.
(3) Cao, Y.; Zhou, H.; Jiang, W.; Chen, C.; Pan, W. *Environ. Sci. Technol.* **2010**, *44*, 3429.
(4) Kikuchi, R. *Environ. Manage.* **2001**, *27*, 837.
(5) (a) Mitsui, Y.; Imada, N.; Kikkawa, H.; Katagawa, A. *Int. J. Greenhouse Gas Control* **2011**, *5*, S143. (b) Zhong, J.; Kumar, M.; Francisco, J. S.; Zeng, X. C. *Acc. Chem. Res.* **2018**, *51*, 1229.
(6) Stockwell, W. R.; Calvert, J. G. *Atmos. Environ.* **1983**, *17*, 2231.
(7) (a) Mauldin, R. L., III; Berndt, T.; Sipilä, M.; Paasonen, P. *Nature* **2012**, *488*, 193. (b) Zhong, J.; Zhu, C.; Li, L.; Richmond, G. L.; Francisco, J. S.; Zeng, X. C. *J. Am. Chem. Soc.* **2017**, *139*, 17168.
(8) Fleig, D.; Vainio, E.; Andersson, K.; Brink, A.; Johnsson, F.; Hupa, M. *Energy Fuels* **2012**, *26*, 5537.
(9) Sipilä, M.; Berndt, T.; Petäjä, T.; Brus, D.; Vanhanen, J.; Stratmann, F.; Patokoski, J.; Hyvärinen, A. P.; Lihavainen, H. *Science* **2010**, *327*, 1243.
(10) Mackenzie, R. B.; Dewberry, C. T.; Leopold, K. R. *Science* **2015**, *349*, 58.
(11) England, G. C.; Zielinska, B.; Loos, K.; Crane, I.; Ritter, K. *Fuel Process. Technol.* **2000**, *65*−*66*, 177.
(12) Li, L.; Kumar, M.; Zhu, C.; Zhong, J.; Francisco, J. S.; Zeng, X. C. *J. Am. Chem. Soc.* **2016**, *138*, 1816.
(13) Renard, J. J.; Calidonna, S. E.; Henley, M. V. *J. Hazard. Mater.* **2004**, *108*, 29.
(14) Zhang, R.; Khalizov, A.; Wang, L.; Hu, M.; Xu, W. *Chem. Rev.* **2012**, *112*, 1957.
(15) Pöschl, U. *Angew. Chem., Int. Ed.* **2005**, *44*, 7520.
(16) Zhang, R.; Wang, G.; Guo, S.; Zamora, M. L.; Ying, Q.; Lin, Y.; Wang, W.; Hu, M.; Wang, Y. *Chem. Rev.* **2015**, *115*, 3803.
(17) Pöschl, U.; Shiraiwa, M. *Chem. Rev.* **2015**, *115*, 4440.
(18) Haywood, J.; Boucher, O. *Rev. Geophys.* **2000**, *38*, 513.
(19) Lohmann, U.; Feichter, J. *Atmos. Chem. Phys.* **2005**, *5*, 715.
(20) Kulmala, M.; Petäjä, T.; Ehn, M.; Thornton, J.; Sipilä, M.; Worsnop, D. R.; Kerminen, V. M. *Annu. Rev. Phys. Chem.* **2014**, *65*, 21.
(21) Kolb, C. E.; Jayne, J. T.; Worsnop, D. R.; Molina, M. J.; Meads, R. F.; Viggiano, A. A. *J. Am. Chem. Soc.* **1994**, *116*, 10314.

DOI: 10.1021/jacs.8b04928
J. Am. Chem. Soc. 2018, 140, 11020−11028

(22) Morokuma, K.; Muguruma, C. *J. Am. Chem. Soc.* **1994**, *116*, 10316.
(23) Jayne, J. T.; Pöschl, U.; Chen, Y. M.; Dai, D.; Molina, L. T.; Worsnop, D. R.; Kolb, C. E.; Molina, M. J. *J. Phys. Chem. A* **1997**, *101*, 10000.
(24) Torrent-Sucarrat, M.; Francisco, J. S.; Anglada, J. M. *J. Am. Chem. Soc.* **2012**, *134*, 20632.
(25) Hazra, M. K.; Sinha, A. *J. Am. Chem. Soc.* **2011**, *133*, 17444.
(26) Bandyopadhyay, B.; Kumar, P.; Biswas, P. *J. Phys. Chem. A* **2017**, *121*, 3101.
(27) Battye, W. H.; Bray, C. D.; Aneja, V. P.; Tong, D.; Lee, P.; Tang, Y. *Atmos. Environ.* **2017**, *163*, 65.
(28) Shen, G.; Suto, M.; Lee, L. C. *J. Geophys. Res.* **1990**, *95*, 13981.
(29) Lovejoy, E. R.; Hanson, D. R. *J. Phys. Chem.* **1996**, *100*, 4459.
(30) Hirota, K.; Mäkelä, J.; Tokunaga, O. *Ind. Eng. Chem. Res.* **1996**, *35*, 3362.
(31) Kim, T. O.; Ishida, T.; Adachi, M.; Okuyama, K.; Seinfeld, J. H. *Aerosol Sci. Technol.* **1998**, *29*, 111.
(32) Shi, Z.; Ford, J. V.; Castleman, A. W. *Chem. Phys. Lett.* **1994**, *220*, 274.
(33) Kumar, M.; Sinha, A.; Francisco, J. S. *Acc. Chem. Res.* **2016**, *49*, 877.
(34) Wong, M. W.; Wiberg, K. B.; Frisch, M. J. *J. Am. Chem. Soc.* **1992**, *114*, 523.
(35) Larson, L. J.; Tao, F. M. *J. Phys. Chem. A* **2001**, *105*, 4344.
(36) Bork, N.; Elm, J.; Olenius, T.; Vehkamäki, H. *Atmos. Chem. Phys.* **2014**, *14*, 12023.
(37) Li, H.; Zhang, X. H.; Zhong, J.; Liu, L.; Zhang, H. J.; Chen, F.; Li, Z. S.; Li, Q. S.; Ge, M. F. *Atmos. Environ.* **2018**, *189*, 244.
(38) Sheng, X.; Zhao, H.; Du, L. *Chemosphere* **2017**, *186*, 331.
(39) Elm, J.; Fard, M.; Bilde, M.; Mikkelsen, V. K. *J. Phys. Chem. A* **2013**, *117*, 12990.
(40) Cappa, C. *Nature* **2016**, *533*, 478.
(41) Bianchi, F.; Trostl, J.; Junninen, H.; Frege, C.; Henne, S.; Hoyle, C. R.; Molteni, U.; Herrmann, E.; Adamov, A.; Bukowiecki, N.; Chen, X.; Duplissy, J.; Gysel, M.; Hutterli, M.; Kangasluoma, J.; Kontkanen, J.; Kurten, A.; Manninen, H. E.; Munch, S.; Perakyla, O.; Petaja, T.; Rondo, L.; Williamson, C.; Weingartner, E.; Curtius, J.; Worsnop, D. R.; Kulmala, M.; Dommen, J.; Baltensperger, U. *Science* **2016**, *352*, 1109.
(42) Molteni, U.; Bianchi, F.; Klein, F.; El Haddad, I.; Frege, C.; Rossi, M. J.; Dommen, J.; Baltensperger, U. *Atmos. Chem. Phys.* **2018**, *18*, 1909.
(43) Kurten, A.; Bergen, A.; Heinritzi, M.; Leiminger, M.; Lorenz, V.; Piel, F.; Simon, M.; Sitals, R.; Wagner, A. C.; Curtius, J. *Atmos. Chem. Phys.* **2016**, *16*, 12793.
(44) Sipila, M.; Sarnela, N.; Jokinen, T.; Henschel, H.; Junninen, H.; Kontkanen, J.; Richters, S.; Kangasluoma, J.; Franchin, A.; Perakyla, O.; Rissanen, M. P.; Ehn, M.; Vehkamaki, H.; Kurten, T.; Berndt, T.; Petaja, T.; Worsnop, D.; Ceburnis, D.; Kerminen, V. M.; Kulmala, M.; O'Dowd, C. *Nature* **2016**, *537*, 532.
(45) Dawson, M. L.; Varner, M. E.; Perraud, V.; Ezell, M. J.; Gerber, R. B.; Finlayson-Pitts, B. J. *Proc. Natl. Acad. Sci. U. S. A.* **2012**, *109*, 18719.
(46) Zhang, R.; Molina, M. J. *Proc. Natl. Acad. Sci. U. S. A.* **2007**, *104*, 5295.
(47) Zhang, R.; Wang, L.; Khalizov, A. F.; Zhao, J.; Zheng, J.; Mcgraw, R. L.; Molina, L. T. *Proc. Natl. Acad. Sci. U. S. A.* **2009**, *106*, 17650.
(48) Yao, L.; Garmash, O.; Bianchi, F.; Zheng, J.; Yan, C.; Kontkanen, J.; Junninen, H.; Mazon, B. S.; Ehn, M.; Paasonen, P.; Sipilä, M.; Wang, M.; Wang, X.; Xiao, S.; Chen, H.; Lu, Y.; Zhang, B.; Wang, D.; Fu, Q.; Geng, F.; Li, L.; Wang, H.; Qiao, L.; Yang, X.; Chen, J.; Kerminen, V.; Petäjä, T.; Worsnop, D.; Kulmala, M.; Wang, L. *Science* **2018**, *361*, 278.
(49) Guo, S.; Hu, M.; Zamora, M. L.; Peng, J.; Shang, D.; Zheng, J.; Du, Z.; Wu, Z.; Shao, M.; Zeng, L. *Proc. Natl. Acad. Sci. U. S. A.* **2014**, *111*, 17373.
(50) Kulmala, M.; Kerminen, V. M.; Petäjä, T.; Ding, A. J.; Wang, L. *Faraday Discuss.* **2017**, *200*, 271.
(51) Almeida, J.; Schobesberger, S.; Kürten, A.; Ortega, I. K.; Kupiainenmäättä, O.; Praplan, A. P.; Adamov, A.; Amorim, A.; Bianchi, F.; Breitenlechner, M. *Nature* **2013**, *502*, 359.
(52) Riccobono, F.; Schobesberger, S.; Scott, C. E.; Dommen, J.; Ortega, I. K.; Rondo, L.; Almeida, J.; Amorim, A.; Bianchi, F.; Breitenlechner, M. *Science* **2014**, *344*, 717.
(53) Kirkby, J.; Duplissy, J.; Sengupta, K.; Frege, C.; Gordon, H.; Williamson, C.; Heinritzi, M.; Simon, M.; Yan, C.; Almeida, J. *Nature* **2016**, *533*, 521.
(54) Mcgrath, M. J.; Olenius, T.; Ortega, I. K.; Loukonen, V.; Paasonen, P.; Kurtén, T.; Kulmala, M.; Ki, H. V. *Atmos. Chem. Phys.* **2012**, *12*, 2345.
(55) Frisch, M. J.; Trucks, G. W.; Schlegel, H. B.; Scuseria, G. E.; Robb, M. A.; Cheeseman, J. R.; Scalmani, G.; Barone, V.; Mennucci, B.; Petersson, G. A.; Nakatsuji, H.; Caricato, M.; Li, X.; Hratchian, H. P.; Izmaylov, A. F.; Bloino, J.; Zheng, G.; Sonnenberg, J. L.; Hada, M.; Ehara, M.; Toyota, K.; Fukuda, R.; Hasegawa, J.; Ishida, M.; Nakajima, T.; Honda, Y.; Kitao, O.; Nakai, H.; Vreven, T.; Montgomery, J. A., Jr.; Peralta, J. E.; Ogliaro, F.; Bearpark, M.; Heyd, J. J.; Brothers, E.; Kudin, K. N.; Staroverov, V. N.; Keith, T.; Kobayashi, R.; Normand, J.; Raghavachari, K.; Rendell, A.; Burant, J. C.; Iyengar, S. S.; Tomasi, J.; Cossi, M.; Rega, N.; Millam, J. M.; Klene, M.; Knox, J. E.; Cross, J. B.; Bakken, V.; Adamo, C.; Jaramillo, J.; Gomperts, R.; Stratmann, R. E.; Yazyev, O.; Austin, A. J.; Cammi, R.; Pomelli, C.; Ochterski, J. W.; Martin, R. L.; Morokuma, K.; Zakrzewski, V. G.; Voth, G. A.; Salvador, P.; Dannenberg, J. J.; Dapprich, S.; Daniels, A. D.; Farkas, O.; Foresman, J. B.; Ortiz, J. V.; Cioslowski, J.; Fox, D. J. *Gaussian 09*, revision A.01; Gaussian Inc.: Wallingford, CT, 2009.
(56) Zhao, Y.; Truhlar, D. G. *Theor. Chem. Acc.* **2008**, *120*, 215.
(57) Neese, F. *Wires. Comput. Mol. Sci.* **2012**, *2*, 73.
(58) Knizia, G.; Adler, T. B.; Werner, H. J. *J. Chem. Phys.* **2009**, *130*, 054104.
(59) Peterson, K. A.; Adler, T. B.; Werner, H. J. *J. Chem. Phys.* **2008**, *128*, 084102.
(60) Zhang, J.; Dolg, M. *Phys. Chem. Chem. Phys.* **2016**, *18*, 3003.
(61) Jorgensen, W. L.; Chandrasekhar, J.; Madura, J. D.; Impey, R. W.; Klein, M. L. *J. Chem. Phys.* **1983**, *79*, 926.
(62) Wales, D. J.; Hodges, M. P. *Chem. Phys. Lett.* **1998**, *286*, 65.
(63) MacKerell, A. D.; Bashford, D.; Bellott, M.; Dunbrack, R. L.; Evanseck, J. D.; Field, M. J.; Fischer, S.; Gao, J.; Guo, H. *J. Phys. Chem. B* **1998**, *102*, 3586.
(64) Stewart, J. J. P. *J. Comput.-Aided Mol. Des.* **1990**, *4*, 1.
(65) Stewart, J. J. P.. *MOPAC2016*, version 16; Stewart Computational Chemistry: Colorado Springs, CO, 2016.
(66) Shampine, L. F.; Reichelt, M. W. *Siam J. Sci. Comput.* **1997**, *18*, 1.
(67) Friedlander, S. K. *Phys. Today* **1977**, *37*, 1116.
(68) Chapman, S.; Cowling, T. G.; Burnett, D. In *The Mathematical Theory of Non-uniform Gases*; Burnett, D., Ed.; Cambridge University Press: Cambridge, 1970.
(69) Lu, T.; Chen, F. *J. Comput. Chem.* **2012**, *33*, 580.
(70) Li, H.; Kupiainen-Määttä, O.; Zhang, H. J.; Zhang, X. H.; Ge, M. F. *Atmos. Environ.* **2017**, *166*, 479.
(71) Kirkby, J.; Curtius, J.; Almeida, J.; Dunne, E.; Duplissy, J.; Ehrhart, S.; Franchin, A.; Gagne, S.; Ickes, L.; Kuerten, A.; Kupc, A.; Metzger, A.; Riccobono, F.; Rondo, L.; Schobesberger, S.; Tsagkogeorgas, G.; Wimmer, D.; Amorim, A.; Bianchi, F.; Breitenlechner, M.; David, A.; Dommen, J.; Downard, A.; Ehn, M.; Flagan, C. R.; Haider, S.; Hansel, A.; Hauser, D.; Jud, W.; Junninen, H.; Kreissl, F.; Kvashin, A.; Laaksonen, A.; Lehtipalo, K.; Lima, J.; Lovejoy, R. E.; Makhmutov, V.; Mathot, S.; Mikkila, J.; Minginette, P.; Mogo, S.; Nieminen, T.; Onnela, A.; Pereira, P.; Petaja, T.; Schnitzhofer, R.; Seinfeld, H. J.; Sipila, M.; Stozhkov, Y.; Stratmann, F.; Tome, A.; Vanhanen, J.; Viisanen, Y.; Vrtala, A.; Wagner, E. P.; Walther, H.; Weingartner, E.; Wex, H.; Winkler, M. P.; Carslaw, S. K.;

DOI: 10.1021/jacs.8b04928
J. Am. Chem. Soc. 2018, 140, 11020−11028

Worsnop, R. D.; Baltensperger, U.; Kulmala, M. *Nature* **2011**, *476*, 429.
(72) Olenius, T.; Kupiainen-Määttä, O.; Ortega, I. K.; Kurtén, T.; Vehkamäki, H. *J. Chem. Phys.* **2013**, *139*, 084312.
(73) Kulmala, M.; Petaja, T.; Monkkonen, P.; Koponen, I. K.; Dal Maso, M.; Aalto, P. P.; Lehtinen, K. E. J.; Kerminen, V. M. *Atmos. Chem. Phys.* **2005**, *5*, 409.
(74) Gao, J.; Chai, F. H.; Wang, T.; Wang, S. L.; Wang, W. X. *J. Environ. Sci.* **2012**, *24*, 14.
(75) Xiao, S.; Wang, M. Y.; Yao, L.; Kulmala, M.; Zhou, B.; Yang, X.; Chen, J. M.; Wang, D. F.; Fu, Q. Y.; Worsnop, D. R.; Wang, L. *Atmos. Chem. Phys.* **2015**, *15*, 1769.
(76) Fliegl, H.; Glöss, A.; Welz, O.; Olzmann, M.; Klopper, W. *J. Chem. Phys.* **2006**, *125*, 54312.
(77) Iuga, C.; Alvarez-Idaboy, J. R.; Vivier-Bunge, A. *Theor. Chem. Acc.* **2011**, *129*, 209.
(78) Liu, J.; Fang, S.; Wang, Z.; Yi, W.; Tao, F. M.; Liu, J. *Environ. Sci. Technol.* **2015**, *49*, 13112.
(79) Tretyakov, M. Y.; Serov, E. A.; Koshelev, M. A.; Parshin, V. V.; Krupnov, A. F. *Phys. Rev. Lett.* **2013**, *110*, 093001.
(80) Scribano, Y.; Goldman, N.; Saykally, R. J.; Leforestier, C. *J. Phys. Chem. A* **2006**, *110*, 5411.
(81) Sarangi, C.; Tripathi, S. N.; Mishra, A. K.; Goel, A.; Welton, E. J. *J. Geophys. Res. Atmos.* **2016**, *121*, 7936.
(82) Riipinen, I.; Sihto, S. L.; Kulmala, M.; Arnold, F.; Maso, M. D.; Birmili, W.; Saarnio, K.; Teinil, K.; Kerminen, V. M.; Laaksonen, A. *Atmos. Chem. Phys.* **2007**, *7*, 1899.
(83) Ge, X.; Wexler, A. S.; Clegg, S. L. *Atmos. Environ.* **2011**, *45*, 524.
(84) Kurten, A.; Jokinen, T.; Simon, M.; Sipila, M.; Sarnela, N.; Junninen, H.; Adamov, A.; Almeida, J.; Amorim, A.; Bianchi, F.; Breitenlechner, M.; Dommen, J.; Donahue, N. M.; Duplissy, J.; Ehrhart, S.; Flagan, R. C.; Franchin, A.; Hakala, J.; Hansel, A.; Heinritzi, M.; Hutterli, M.; Kangasluoma, J.; Kirkby, J.; Laaksonen, A.; Lehtipalo, K.; Leiminger, M.; Makhmutov, V.; Mathot, S.; Onnela, A.; Petaja, T.; Praplan, A. P.; Riccobono, F.; Rissanen, M. P.; Rondo, L.; Schobesberger, S.; Seinfeld, J. H.; Steiner, G.; Tome, A.; Trostl, J.; Winkler, P. M.; Williamson, C.; Wimmer, D.; Ye, P. L.; Baltensperger, U.; Carslaw, K. S.; Kulmala, M.; Worsnop, D. R.; Curtius, J. *Proc. Natl. Acad. Sci. U. S. A.* **2014**, *111*, 15019.
(85) Kurten, A.; Li, C. X.; Bianchi, F.; Curtius, J.; Dias, A.; Donahue, N. M.; Duplissy, J.; Flagan, R. C.; Hakala, J.; Jokinen, T.; Kirkby, J.; Kulmala, M.; Laaksonen, A.; Lehtipalo, K.; Makhmutov, V.; Onnela, A.; Rissanen, M. P.; Simon, M.; Sipila, M.; Stozhkov, Y.; Trostl, J.; Ye, P. L.; McMurry, P. H. *Atmos. Chem. Phys.* **2018**, *18*, 845.
(86) Zhang, H. J.; Kupiainen-Määttä, O.; Zhang, X. H.; Molinero, V.; Zhang, Y. H.; Li, Z. S. *J. Chem. Phys.* **2017**, *146*, 184308.
(87) Liu, L.; Kupiainen-Määttä, O.; Zhang, H. J.; Li, H.; Zhong, J.; Kurtén, T.; Vehkamäki, H.; Zhang, S. W.; Zhang, Y. H.; Ge, M. F.; Zhang, X. H.; Li, Z. S. *J. Chem. Phys.* **2018**, *148*, 214303.
(88) Liu, L.; Li, H.; Zhang, H. J.; Zhong, J.; Bai, Y.; Ge, M. F.; Li, Z. S.; Chen, Y.; Zhang, X. H. *Phys. Chem. Chem. Phys.* **2018**, *20*, 17406.

DOI: 10.1021/jacs.8b04928
J. Am. Chem. Soc. 2018, 140, 11020−11028